arktos (2020) 6:93–105
https://doi.org/10.1007/s41063-020-00078-9

ORIGINAL ARTICLE

# Zircon geochronology and geochemistry of the Ward Hunt pluton, Pearya terrane, Canadian High Arctic: Insights into its age, origin, and circum-Arctic Timanide connections

**Shawn J. Malone**[1] · **William C. McClelland**[2]

Received: 8 April 2020 / Accepted: 31 July 2020 / Published online: 10 August 2020


**Abstract**
The northern margin of the Neoproterozoic Timanide Orogen is truncated by Paleozoic deformation of the Caledonian Orogen. Evidence for dispersion of terranes affected by the Timanide Orogen is documented through contemporaneous tectonothermal activity, and by detrital zircon in sedimentary rock from across the Arctic Ocean margins. However, directly tying these terranes to the Caledonide realm is hindered by the paucity of appropriate events in proximal terranes. The Ward Hunt Pluton, a previously undated syenite–monzodiorite intrusion located on Ward Hunt Island, northern Pearya terrane, yields a crystallization age of 542 ± 2 Ma. Trace-element data from the igneous zircon suggest that the pluton intruded older metasedimentary rocks of the terrane as part of a volcanic arc system, indicated by juvenile Hf isotopic signatures and trace-element data. The data support links between the Pearya terrane and other Neoproterozoic–Cambrian arc systems, such as those proposed in Arctic Alaska-Chukota and the Alexander terrane.

**Keywords** Pearya terrane · Timanide orogen · Arctic tectonics · Geochronology

## Introduction

The Neoproterozoic Timanide Orogen is an important marker for tracing the evolution of circum-Arctic terranes with ties to Baltica. The orogen is best expressed along the northeastern margin of Baltica, extending from the southern half of the Ural Mountains to Novaya Zemlya (Russia) and the Varanger Peninsula of Norway, where it is truncated by Caledonian deformation [1]. Tectonic activity in the Timanides resulted from subduction directed underneath Baltica, leading to magmatism, metamorphism, and widespread deformation related to the development of a continental arc [2] or the accretion of a continental fragment (e.g., Arctida; [3, 4]). The main pulse of tectonothermal activity occurred between 610 and 560 Ma [5, 6]; however, Roberts and Olovyanishnikov [7] suggest that this activity occurred diachronously along strike, with the northwestern and southeastern parts of the belt characterized by somewhat younger activity. The northern margin of the Timanide Orogen is particularly interesting due to evidence of activity that extends into Svalbard. Torrelian metamorphism at c. 640 Ma is recorded by monazite growth, $^{40}Ar/^{39}Ar$ cooling ages of mica and hornblende, and metamorphic fabric development at several localities in Svalbard's Southwestern terrane [8–11]. The terrane is bounded by large-scale strike–slip faults that Mazur et al. [12] propose separated the Southwestern terrane and a portion of the Pearya terrane on the Canadian Arctic Margin, from the truncated Timanian margin of Baltica. Other distant terranes show evidence of a Timanide Orogen connection, such as Arctic Alaska-Chukotka (e.g., [13–15]) and the Alexander terrane of the Cordillera (e.g., [16, 17]). Many tectonic models exist to explain these connections; however, evidence from terranes proximal to the Caledonian margin is sparse. This study presents data from the previously undated Ward Hunt Pluton, located on Ward Hunt Island in the northernmost exposures of the Pearya terrane (Fig. 1). We suggest that this pluton represents a direct link between the Pearya terrane and the

✉ Shawn J. Malone
malones@uwgb.edu

William C. McClelland
bill-mcclelland@uiowa.edu

[1] Department of Natural & Applied Sciences, University of Wisconsin Green Bay, Green Bay, WI 54311, USA

[2] Department of Earth and Environmental Sciences, University of Iowa, Iowa City, IA 52242, USA

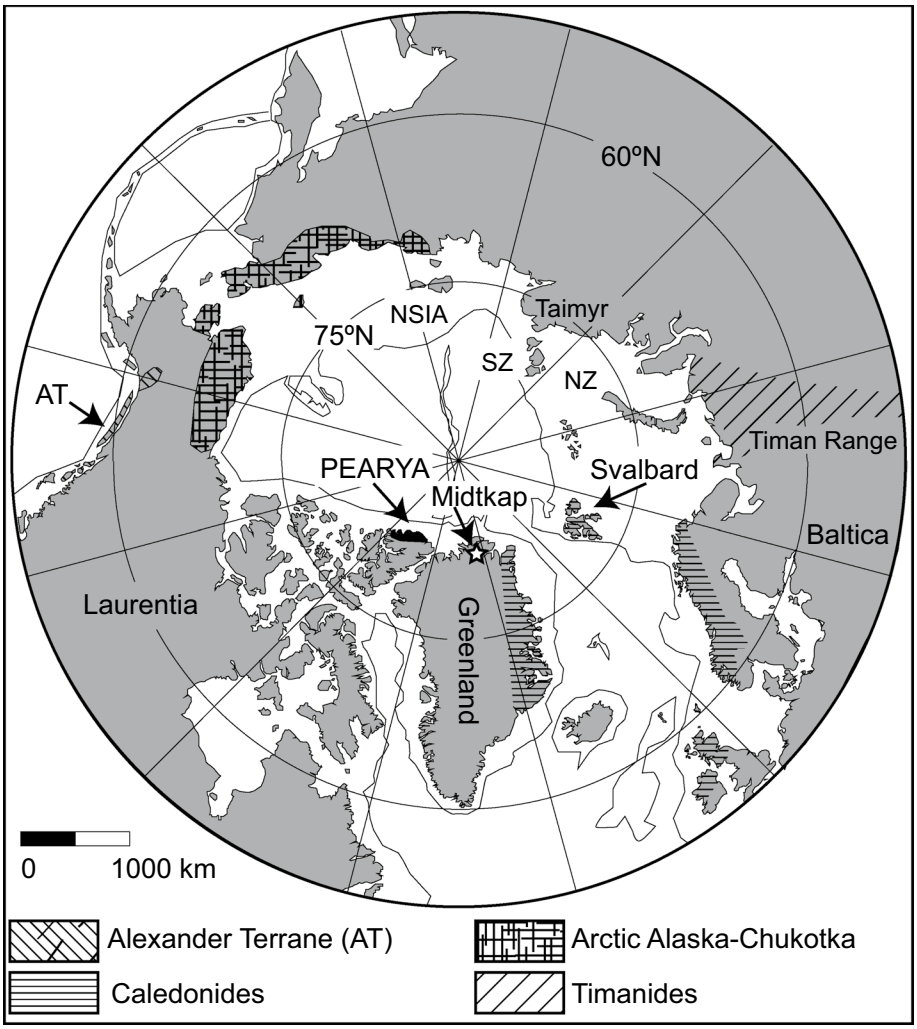


**Fig. 1** The Arctic Ocean region, illustrating important geographic locations to this study. *NZ* Novaya Zemlya, *SZ* Severnya Zemlya, *NSIA* New Siberian Islands Archipelago

Timanide Orogen, helping to fill in the missing link between Svalbard and the more distant terranes to the west.

## Geologic setting

The Pearya terrane is an exotic terrane (e.g., [18–24]) located on the present day northern margin of the Franklinian basin, northernmost Ellesmere Island (Fig. 1). Trettin [19] originally proposed a Caledonian origin for the Pearya terrane and suggested correlation with terranes in Svalbard. The timing of accretion of the Pearya terrane against the Franklinian margin of the Canadian Arctic is still uncertain; however, it is presumed to have occurred between the late Silurian and middle Devonian (e.g., [24] and references therein). Data supporting this interpretation include: the appearance of Pearya-sourced clasts in conglomerates in deep-water basinal rocks of the Silurian Danish River Formation [25]; detrital zircon provenance shifts from a recycled Caledonian orogenic source to a Laurentian cratonic source by the early Carboniferous [24, 26]; metamorphism in the terrane basement observed between c. 395 and 372 Ma [27]; and the emplacement of the Cape Woods post-tectonic pluton at 390 Ma [28]. The terrane was likely emplaced as a series of fault-bound slices, along a series of sinistral strike-slip faults that splay into arcuate thrusts at the southwest end of the terrane [29, 30].

The Pearya terrane is divided into five tectonostratigraphic units labeled Successions I through V (Fig. 2a); [21]. Succession I is comprised of abundant, variably deformed orthogneiss, with minor amphibolite and metasedimentary units. These yield dominantly earliest Neoproterozoic ages [23, 28, 31, 32]. Succession II includes a series of variably metamorphosed Proterozoic siliciclastic and carbonate units, overlain by a Cambrian–Ordovician sequence of clastic, carbonate, and volcanic units. Trettin et al. [28] reported a zircon U–Pb age of 503 + 8/− 2 Ma from a sheared metarhyolite near the top of Succession II. Other age control for Succession II comes from presumed Cryogenian diamictite units, and from fragments of Early Cambrian hexacintnellid

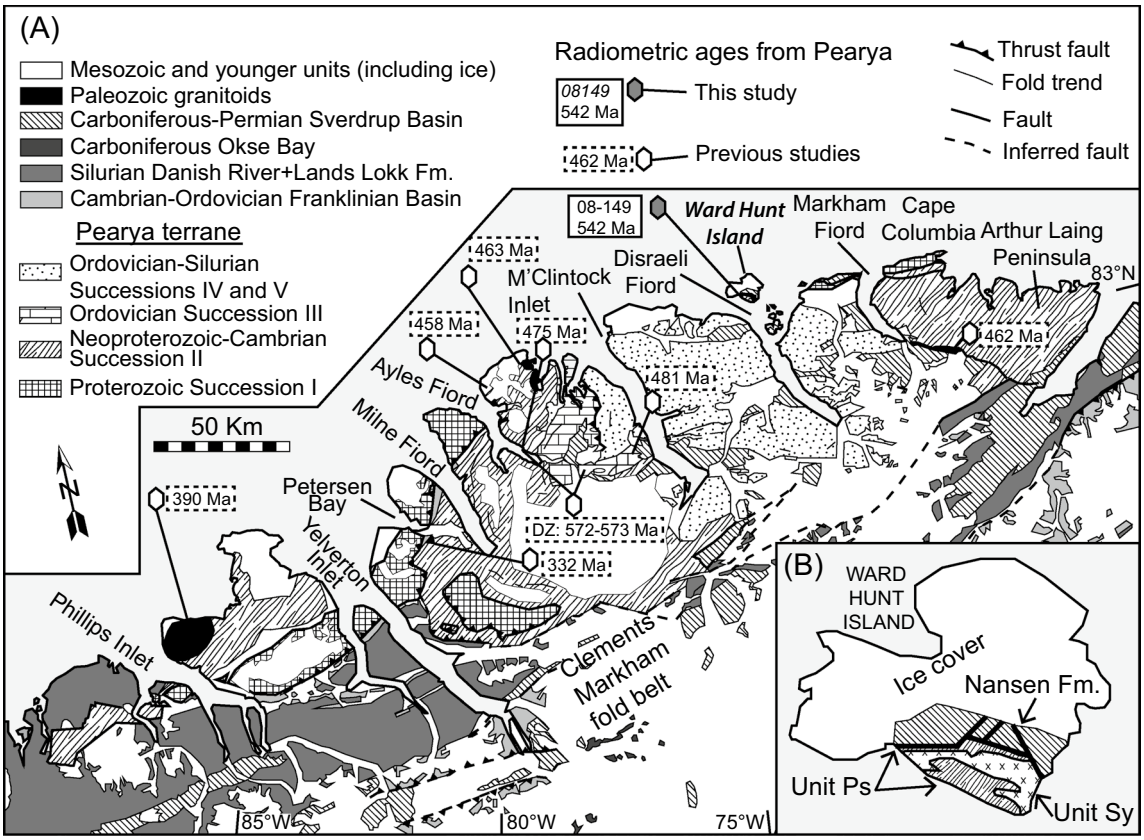


**Fig. 2** **a** Simplified geologic map of northern Ellesmere Island, adapted from Trettin [21] and Mayr [89]. Included is a selection of U–Pb radiometric ages from Paleozoic intrusions and detrital zircon (DZ) components in the Pearya terrane from Trettin et al. [28, 31, 33] and Estrada et al. [32], as well as the sample location of the Ward Hunt Pluton collected in 2008. **b** Geology of Ward Hunt Island, adapted from [21, 89]

sponge spicules [21]. Succession III of the Pearya terrane records Early-to-Middle Ordovician volcanic arc igneous activity and associated arc-margin sedimentation. Two key elements are preserved: The Maskell Inlet Complex, consisting of an intensely deformed and variably metamorphosed volcaniclastic sedimentary sequence hundreds of meters thick, and the Thores suite of ultramafic to granitoid rocks, presumed to represent a sub-arc igneous complex [21, 32]. A U–Pb zircon age from Trettin et al. [32] of 481 + 7/− 6 Ma for the M'Clintock West body places a lower bound on arc accretion during the terrane-scale M'Clintock orogeny [29]. This terrane-scale orogen is responsible for the high angle unconformity that separates Succession II and III from the overlying middle Ordovician to Silurian sedimentary rocks deposited on the Pearya terrane [29]. Succession IV and V are post-M'Clintock orogeny sedimentary units deposited in a variety of settings, ranging from deep marine basinal clastics to shallow marine carbonate environments [21]. These units preserve a record of variable deformation, but little-to-no evidence of metamorphism. Silurian sedimentary rocks of the Danish River Formation in the Clements Markham Fold Belt indicate proximity of the Pearya terrane to the Laurentian margin and subsequent Late Silurian to Early Carboniferous accretion-related deformation of the Ellesmerian Orogen [34–38].

Ward Hunt Island is located near the mouth of Disraeli Fiord off the coast of northern Ellesmere Island, Nunavut, Canada (Fig. 1). The island is underlain by three main bedrock units: metamorphic rocks [Ps], the Ward Hunt Pluton [Sy], and Carboniferous-to-Permian units of the Nansen Formation (Fig. 2b). The metamorphic unit includes schist and phyllite that are composed of biotite, muscovite, chlorite, albitic plagioclase feldspar, and quartz and locally preserve cataclastic textures [39]. The unit is correlated with Succession II on the basis of lithological similarities [21]. The Ward Hunt Pluton is dominated by syenite containing microcline, perthite, and quartz but includes monzodiorite consisting of albite, chlorite, epidote, and hornblende and additional mafic phases commonly altered to green biotite and oxides [39]. Geochemical analysis of the monzodiorite phase reveals a metaluminous chemistry with tectonic discrimination plots placing the Ward Hunt Pluton in the Volcanic Arc Granite field in Rb versus Nb + Y and Rb versus Ta + Yb space [21]. Trettin [21] suggests that the degree of alteration to these rocks makes this

interpretation suspect and correlates the pluton with Succession I. However, the cross-cutting relationship with metamorphic rocks presumed to be correlative with Succession II suggests that the Ward Hunt Pluton is younger than Succession I.

## Methods

Sample 08149 was processed at the University of Iowa mineral separation facility, starting with crushing and pulverization using a BICO badger jaw crusher and disk mill. The resultant material was then washed across a Gemeni GT60 water table to concentrate the dense mineral fraction. Zircon in this fraction was purified by magnetic susceptibility methods and heavy liquid separation in methylene iodide. Individual zircon grains were examined in alcohol and imaged in reflected light, and then picked and mounted in a 2.54 cm epoxy round mount. The mount was polished and cathodoluminescence (CL) imaged at the USGS-Stanford University Ion Probe Laboratory. Zircon U–Pb and trace-element analyses were conducted simultaneously by SIMS (secondary ion mass spectrometry) using the SHRIMP-RG (sensitive high-resolution ion microprobe–reverse geometry) instrument at the USGS-Stanford University Ion Probe Laboratory following methods outlined in Barth and Wooden [40]. Spot sizes were approximately 25 µm in diameter. Fractionation corrections were calibrated by replicate analysis of the zircon standard R33 [421 Ma]; [41, 42]. The U and trace-element concentrations were calibrated with MAD-559 [43]. Data reduction utilized the SQUID-2 add-in to Microsoft Excel [44], with U–Pb ages and concordia plots were generated using Isoplot ver. 3.0, an add-in to Microsoft Excel by Ludwig, [45]. Reported values for Eu* and Ce* are calculated as geometric means using the abundances of the adjacent elements (e.g., $Eu^* = Eu_{normalized}/[[Sm_{normalized} \times Gd_{normalized}]/2]$). The U–Pb data are presented in Table 1, and trace-element data are presented in Table 2. Lu–Hf isotopic analysis of zircon utilized different grains from the zircon fraction. The new grains were mounted in a 2.54 cm epoxy round mount, polished, and CL imaged at the Arizona LaserChron Center. U–Pb analysis identified age domains in the grains, and domains within error of the SHRIMP U–Pb crystallization age were selected for LA-ICPMS (laser ablation-inductively coupled plasma-mass spectrometry) Lu–Hf analysis following the protocols outlined in Gehrels et al. [46, 47] and Cecil et al. [48]. Lu–Hf data are presented in Table 3.

## Results

### Sample description

Sample 08-149 was collected from the syenite phase of the syenite–monzodiorite plutonic complex (Fig. 3a). The syenite is dominated in hand sample by pink potassium feldspar

**Table 1** SIMS U–Pb data for the Ward Hunt Pluton zircon grains

| SHRIMP Spot ID | U (ppm) | Th (ppm) | $^{232}Th/^{238}U$ | $^{206}Pb_c$ | $^{206}Pb^*/^{238}U$ | % error | $^{207}Pb^*/^{206}Pb^*$ | % error | $^{207}$ Pb corr $^{206}Pb/^{238}U$ age | 1σ error | $^{204}$Pb corr $^{207}Pb/^{206}Pb$ age | 1σ error |
|---|---|---|---|---|---|---|---|---|---|---|---|---|
| 08-149-1.1 | 439 | 210 | 0.49 | − 0.12 | 14.88 | 0.4 | 0.0619 | 0.8 | 415.9 | 1.5 | 571 | 30 |
| 08-149-2.1 | 683 | 165 | 0.25 | 0.14 | 13.40 | 0.6 | 0.0658 | 1.3 | 458.8 | 2.8 | 479 | 78 |
| 08-149-3.1 | 669 | 497 | 0.77 | 0.09 | 12.60 | 0.4 | 0.0592 | 0.8 | 491.1 | 1.7 | 531 | 23 |
| 08-149-4.1 | 694 | 87 | 0.13 | − 0.02 | 12.17 | 0.5 | 0.0586 | 1.0 | 508.3 | 2.3 | 543 | 24 |
| 08-149-5.1 | 253 | 197 | 0.80 | 1.13 | 12.00 | 0.3 | 0.0598 | 0.7 | 514.6 | 1.7 | 577 | 21 |
| 08-149-6.1 | 408 | 406 | 1.03 | − 0.10 | 11.63 | 0.4 | 0.0594 | 1.1 | 530.9 | 2.1 | 535 | 32 |
| 08-149-7.1 | 481 | 570 | 1.22 | 2.01 | 11.62 | 0.5 | 0.0578 | 1.0 | 532.2 | 2.5 | 558 | 27 |
| 08-149-8.1 | 475 | 420 | 0.91 | 0.03 | 11.60 | 0.3 | 0.0576 | 0.7 | 533.5 | 1.7 | 522 | 16 |
| 08-149-9.1 | 379 | 136 | 0.37 | 0.08 | 11.58 | 0.4 | 0.0588 | 0.8 | 533.6 | 1.9 | 566 | 18 |
| 08-149-10.1 | 638 | 381 | 0.62 | 0.11 | 11.50 | 0.4 | 0.0583 | 0.8 | 537.5 | 2.0 | 506 | 24 |
| 08-149-11.1 | 905 | 677 | 0.77 | − 0.03 | 11.18 | 0.5 | 0.0747 | 4.6 | 541.5 | 3.3 | 548 | 190 |
| 08-149-12.1 | 553 | 115 | 0.21 | 0.15 | 11.39 | 0.4 | 0.0584 | 0.8 | 542.6 | 1.9 | 545 | 17 |
| 08-149-13.1 | 777 | 180 | 0.24 | 0.06 | 11.36 | 0.5 | 0.0579 | 1.6 | 544.3 | 2.7 | 503 | 37 |
| 08-149-14.1 | 704 | 133 | 0.19 | 0.00 | 11.33 | 0.4 | 0.0579 | 0.8 | 545.4 | 2.0 | 501 | 22 |
| 08-149-15.1 | 671 | 246 | 0.38 | 0.34 | 11.34 | 0.5 | 0.0577 | 1.0 | 545.1 | 2.5 | 547 | 27 |

**Table 2** SIMS trace-element data (in ppm) for the Ward Hunt Pluton zircon grains

| Spot ID | La | Ce | Nd | Sm | Eu | Gd | Dy | Er | Yb | Hf | Y | Th | U |
|---|---|---|---|---|---|---|---|---|---|---|---|---|---|
| 08149-15.1 | 16.62 | 80.4 | 23.2 | 11.3 | 14.8 | 44 | 114.6 | 124.6 | 88.4 | 8331 | 995 | 250 | 638 |
| 08149-2.1 | 1.56 | 16.1 | 3.9 | 3.1 | 3.7 | 15 | 51.3 | 78.2 | 64.4 | 7959 | 567 | 167 | 645 |
| 08149-5.1 | 3.44 | 22.8 | 4.8 | 4.5 | 5.5 | 24 | 98.1 | 142.4 | 140.1 | 9172 | 969 | 205 | 247 |
| 08149-4.1 | 0.07 | 6.2 | 0.2 | 0.5 | 0.4 | 6 | 30.3 | 54.3 | 45.4 | 8925 | 357 | 88 | 660 |
| 08149-+654/13.1 | 2.90 | 23.9 | 5.6 | 2.9 | 3.5 | 13 | 55.3 | 89.6 | 71.8 | 8982 | 608 | 186 | 753 |
| 08149-8.1 | 0.46 | 68.3 | 3.8 | 9.9 | 6.0 | 109 | 437.0 | 489.9 | 308.7 | 10,860 | 4020 | 419 | 443 |
| 08,149–1.1 | 0.01 | 10.2 | 0.1 | 0.6 | 0.3 | 9 | 55.9 | 95.6 | 76.6 | 8167 | 721 | 217 | 426 |
| 08149-12.1 | 2.01 | 13.3 | 3.2 | 2.4 | 2.2 | 8 | 30.8 | 54.0 | 47.1 | 8336 | 373 | 117 | 529 |
| 08149-11.1 | 0.20 | 37.7 | 1.7 | 3.1 | 3.2 | 36 | 183.0 | 269.1 | 218.6 | 8418 | 1991 | 692 | 870 |
| 08149-6.1 | 0.02 | 40.8 | 1.8 | 5.7 | 2.7 | 72 | 295.6 | 353.9 | 226.8 | 9878 | 2829 | 419 | 396 |
| 08149-3.1 | 0.06 | 31.1 | 0.7 | 2.2 | 1.1 | 32 | 166.5 | 253.1 | 171.6 | 7909 | 1946 | 507 | 642 |
| 08149-10.1 | 0.03 | 24.3 | 0.5 | 1.5 | 0.9 | 22 | 118.6 | 162.4 | 115.3 | 10,330 | 1228 | 391 | 619 |
| 08149-14.1 | 0.09 | 7.8 | 0.1 | 0.3 | 0.3 | 5 | 36.2 | 67.7 | 55.3 | 9859 | 460 | 137 | 688 |
| 08149-7.1 | 1.52 | 59.2 | 5.4 | 10.0 | 6.3 | 100 | 415.4 | 488.2 | 309.5 | 10,614 | 3920 | 580 | 461 |
| 08149-9.1 | 0.02 | 14.4 | 0.5 | 1.6 | 0.9 | 20 | 95.7 | 131.2 | 79.1 | 8417 | 985 | 141 | 374 |

**Table 3** LA-ICPMS Lu/Hf data for the Ward Hunt Pluton zircon grains

| LA–ICPMS Spot ID | $(^{176}Yb + {}^{176}Lu)/^{176}Hf$ (%) | $^{176}Hf/^{177}Hf$ | $\pm(1\sigma)$ | $^{176}Lu/^{177}Hf$ | $^{176}Hf/^{177}Hf(T)$ | εHf (0) | εHf (0) $\pm(1\sigma)$ | εHf($T$) | U/Pb age ($T$—Ma) |
|---|---|---|---|---|---|---|---|---|---|
| 08-149-1 | 19.846646 | 0.282571 | 0.000085 | 0.000671 | 0.282564 | − 7.6 | 3.0 | 4.3 | 542 |
| 08-149-11 | 8.433587 | 0.282563 | 0.000083 | 0.000294 | 0.282560 | − 7.9 | 2.9 | 4.1 | 542 |
| 0-–149-12 | 18.870782 | 0.282708 | 0.000064 | 0.000656 | 0.282702 | − 2.7 | 2.3 | 9.2 | 542 |
| 08-149-13 | 8.348406 | 0.282620 | 0.000066 | 0.000297 | 0.282617 | − 5.8 | 2.3 | 6.2 | 542 |
| 08-149-14 | 23.214854 | 0.282580 | 0.000061 | 0.000755 | 0.282572 | − 7.3 | 2.2 | 4.6 | 542 |
| 08-149-17 | 18.469918 | 0.282620 | 0.000078 | 0.000636 | 0.282614 | − 5.8 | 2.8 | 6.1 | 542 |
| 08-149-6 | 12.064425 | 0.282735 | 0.000071 | 0.000447 | 0.282730 | − 1.8 | 2.5 | 10.2 | 542 |
| 08-149-8 | 18.945968 | 0.282413 | 0.000090 | 0.000812 | 0.282404 | − 13.2 | 3.2 | − 1.4 | 542 |

U/Pb age (T) assigned based on the concordia age from SIMS analyses

and an altered greenish-black mafic phase (Fig. 3b). Thin section analysis (Fig. 4a) revealed that the feldspar is variably altered, with some grains cloudy due to sericite. The mafic phase, interpreted as an amphibole group mineral, is also altered to biotite, chlorite, and opaque phases (Fig. 4b).

## SIMS results: U–Pb and trace elements

Fifteen individual zircon grains separated from sample 08-149 were analyzed at the USGS-Stanford University Ion Probe Laboratory. Zircon from sample 08-149 consists of blocky, brown, turbid grains and fragments that range in size from 100 to 300 µm in length (Fig. 5a). CL images reveal that mottled zones, sometimes rich in inclusions, dominate most of the grains; however, some grains contained domains of oscillatory growth zonation interpreted to be of igneous origin (Fig. 5b). Trace-element patterns (Fig. 6) between the grains was variable, with some showing elevated light REE and others showing depressed heavy REE characteristics. Values for Yb/Gd range from 3.1 to 10.2, reflecting a flatter heavy REE segment of the pattern. Negative Eu anomalies are indicated by Eu/Eu* values of 0.40–0.90, and positive Ce anomalies are indicated by values of 2.1 to 144.1. U and Th concentrations varied with U ranging from 253 to 777 ppm and Th from 87 to 570 ppm. Th/U ratios ranged from 0.13 to 1.22. The zircon grains yielded a range of common Pb corrected $^{206}Pb/^{238}U$ ages from 417 to 545 Ma. Several of the young zircon show elevated light REE values indicating open system behavior [49]. Other young grains show normal REE patterns, but plot along a Pb-loss trajectory on a Tera-Wasserburg concordia diagram (Fig. 7a). The six oldest grains yield a weighed mean $^{206}Pb/^{238}U$ age of 542 ± 2 [MSWD = 2] and a concordia age of 542 ± 2 [MSWD = 2.9] which is interpreted as the emplacement age for the Ward Hunt Pluton (Fig. 7b).

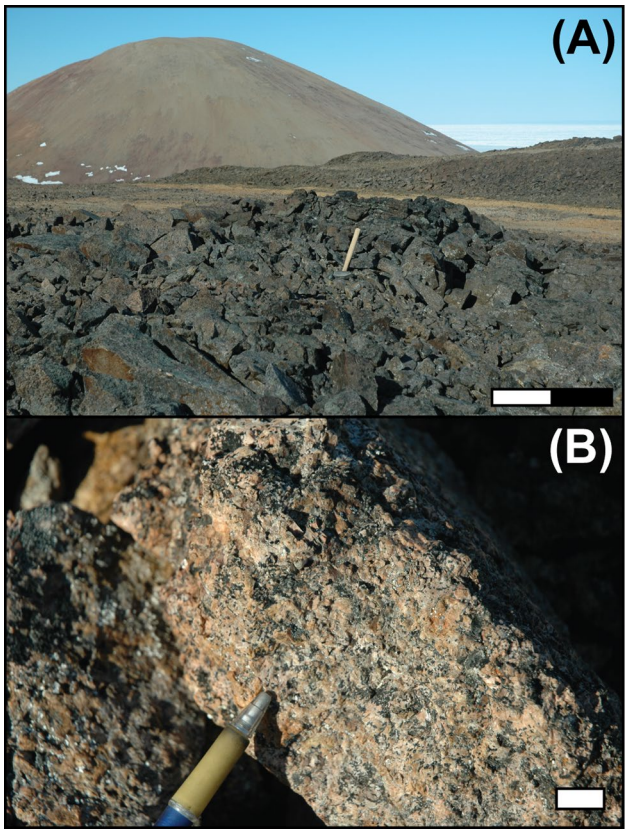


**Fig. 3** Sample photographs. **a** Field photograph of the pluton on Ward Hunt Island, showing the sample outcrop. The scale bar is approximately 1 m in length. **b** Close-up view of the sample collected for this study. The scale bar is approximately 1 cm

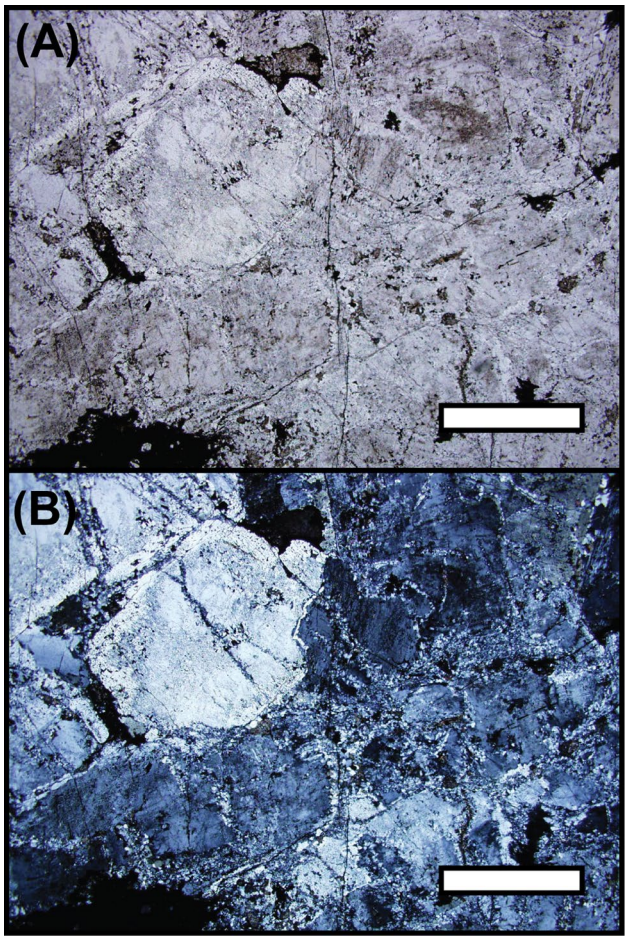


**Fig. 4** Representative photomicrographs of the sample. **a** Plane polarized light. **b** Cross-polarized light. Scale bar is approximately 1 mm

### LA-ICPMS results: Lu–Hf isotope geochemistry

Additional zircon grains were mounted, CL imaged, and analyzed by LA-ICPMS for U–Pb and Lu–Hf isotopic data at the Arizona LaserChron Center. Six zircon, yielding $^{206}Pb/^{238}U$ ages from c. 535 to c. 547 Ma, were chosen for Lu–Hf isotopic analysis. $^{176}Hf/^{177}Hf$ values ranged from 0.282563 to 0.282708, yielding $\varepsilon Hf_{[t]}$ values of + 4.1 to + 9.2. All analyses define an average $\varepsilon Hf_{[t]}$ value of + 5.7 for the Ward Hunt Pluton.

## Discussion

### Age and tectonic setting of the Ward Hunt Pluton

Zircon U–Pb analysis yields an age of 542 ± 2 Ma for the Ward Hunt Pluton, consistent with the observed field relationships outlined by Trettin [21]. This age reveals a previously poorly constrained magmatic event in the Pearya terrane. Succession I orthogneiss units yield early Neoproterozoic ages and are interpreted to represent a continental arc system [23]. There are little geochemical data available for the sheared rhyolite in Succession II that yielded a zircon U–Pb age of c. 503 Ma [28] to establish the its tectonic affinity. The majority of Paleozoic intrusions from the Pearya terrane define Ordovician–early Silurian and middle–late Devonian magmatism (Fig. 2); [31, 32] and references therein], reflecting the well-documented links between Pearya and the Caledonian and Ellesmerian orogenies.

The tectonic setting of the Ward Hunt Pluton is uncertain; however, zircon trace element and Lu–Hf geochemistry help to illuminate the processes affecting its evolution and narrow the origin of the primary magma. The range of observed Th/U values is generally indicative of juvenile magma input rather than solely crustal melts (e.g., [50]). In addition, the low Th/U suggests that the host syenite is not A-type granitoid [51]. Yb/Gd values are a proxy for magma evolution by fractional crystallization, where middle REE are typically removed by accessory phases such as apatite and titanite [40]. Th/U vs. Yb/Gd (Fig. 8a) displays a fractionation trend, but over a limited time of zircon growth suggestive

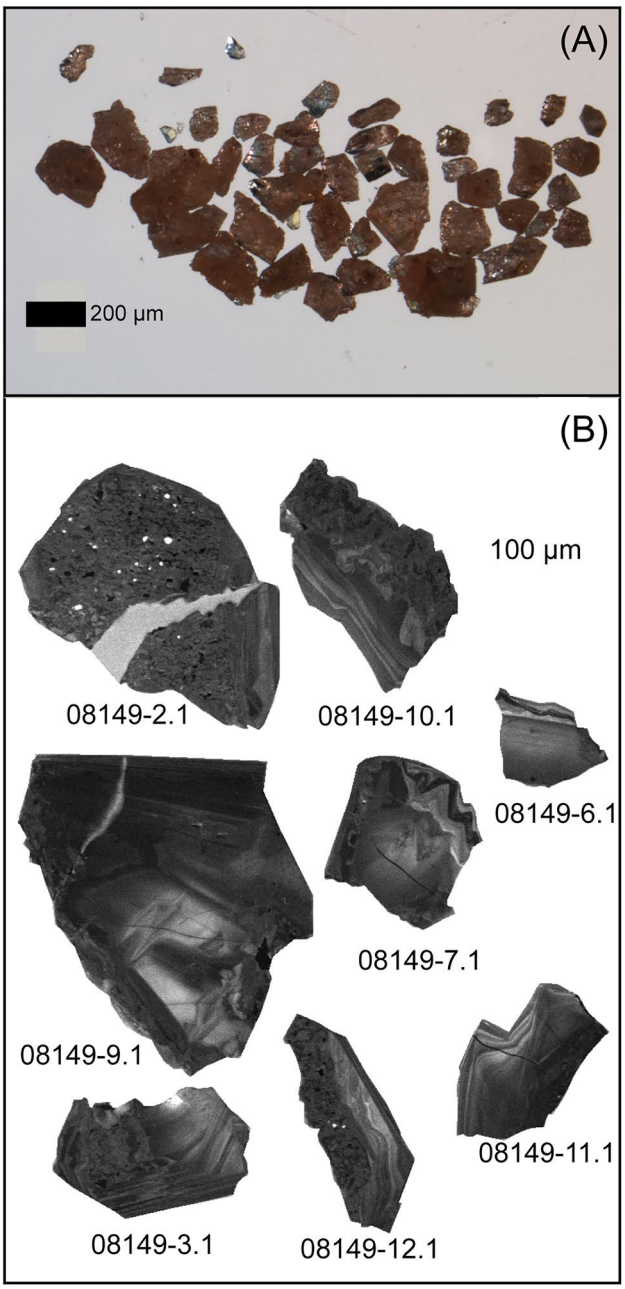


**Fig. 5** Zircon images. **a** Reflected light image of zircon grains separated from sample 08149. **b** Cathodoluminescence (CL) images of selected zircon. Many grains showed mottled domains believed to represent metamict zones, as well as areas of primary igneous oscillatory zoning. Spot sizes, indicated by open white circles, are approximately 25 µm in diameter

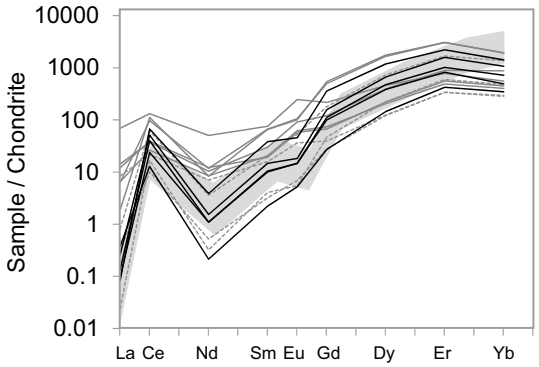


**Fig. 6** Chondrite normalized REE plot for sample 08149 zircon. Black lines are data from grains showing low degrees of disturbance. Gray lines are analyses rejected in age calculation due to elevated LREE (solid) or Pb loss (dashed). Most of the rejected analyses show elevated LREE patterns and Pb loss typical of disturbed zircon (solid) or just showed evidence of Pb loss during U–Pb analysis (dashed). Gray field is REE pattern for typical igneous zircon from R33 analyzed during the SIMS analytical session

of limited inheritance from long-lived magmatic system. Ce/Sm and Eu/Eu* can track magma oxidation conditions [49]. When plotted against Yb/Gd (Fig. 8b, c), the Ce/Sm and Eu/Eu* variations indicate that fractional crystallization played less of a role in the magma evolution than varying oxidation conditions. This may be due to the minor input of anatectic fluid into the original magma. This is further suggested by the trend observed on the Th ppm vs U/Ce plot (Fig. 8d). While the Ward Hunt Pluton zircon analyses plot in the magmatic field, the negative trend defined by the data points may indicate that a small input of anatectic fluid did affect the magma (and perhaps oxidation conditions) during crystallization. Hf concentrations serve as another proxy for magma evolution. Hf concentration plotted against U/Yb provides another means to discriminate magma fractionation from source enrichments [52]. The Ward Hunt Pluton suite reveals a trend dominated by the source region, again downplaying the role of magma evolution in the chemical characteristics of the zircon (Fig. 8e). Grimes et al. [52] include a tectonic discrimination plot based on Gd/Yb variations against U/Yb. Zircon from the Ward Hunt Pluton plots outside of most categories; however, this may reflect the influence of garnet at depth in a continental arc setting (Fig. 8f). The $\varepsilon Hf_{[t]}$ values of +4.1 to +9.2 suggest that the original source was relatively juvenile, with only limited crustal input (Fig. 9). When taken in sum, these data suggest that the Ward Hunt Pluton formed in a volcanic arc setting at c. 542 Ma, providing a link between the Pearya terrane, the larger Timanide Orogen, and Circum-Arctic terranes with Timanian affinities.

## The Ward Hunt Pluton and Circum-Arctic Timanide connections

The influence of the Timanide Orogen extends from the classic sections on the northeastern margin of Baltica to the Arctic Alaska-Chukotka terrane and other Cordilleran terranes that originated at peri-Baltican subduction zones [53–56]. The detrital zircon signature from the Timanide Orogen is dominated by ages ranging from 650 to 525 Ma, and has been well documented from the Timan Range, northern

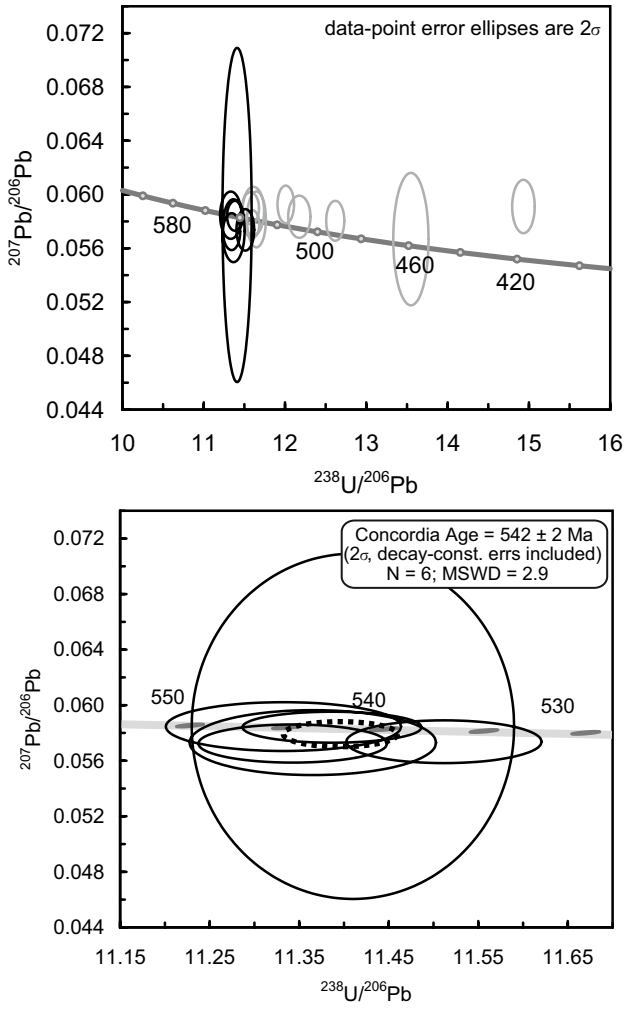


**Fig. 7** Zircon U–Pb age data. **a** Tera-Waserberg concordia diagram of all zircon U/Pb analyses. Data are corrected for common Pb, and error ellipses are illustrated at 2$\sigma$. Gray ellipses are analyses rejected from the age calculation due to Pb loss. **b** Tera-Waserberg concordia diagram for zircon U/Pb analyses used for age calculation. These data are corrected for common Pb, and error ellipses are at 2$\sigma$. Concordia age is represented by the dashed black ellipse

Taimyr, Novaya Zemlya, Severnya Zemlya, and the New Siberian Islands Archipelago (Fig. 1); [5, 57–61]. The c. 542 Ma age from the Ward Hunt Pluton is older than previously documented tectonothermal events in the Pearya terrane; however, probable volcanic arc activity in Succession III at this time and other lines of evidence supports a link between the Timanides and portions of the Pearya terrane [32]. Evidence for pre-Carboniferous sinistral strike–slip displacement documented in the Pearya terrane and Svalbard (e.g., [12, 30, 62, 63]) is consistent with the models of large-scale terrane translation through the Arctic (e.g., [53]) as well as Caledonian escape models for the Pearya terrane [64]. These models provide a regional-scale mechanism to juxtapose the Ward Hunt Pluton and its wall rocks with other units of the Pearya terrane prior to or during its accretion along the northern margin of Laurentia and separate it from other Timanide terranes displaced to the Cordilleran margin.

Detrital zircon U–Pb age data from Proterozoic Succession II units of the Pearya terrane yield a small population of ages consistent with a Timanide source area [22, 32]. While generally older than the Ward Hunt Pluton, the detrital zircon age data from Succession II and III of the Pearya terrane independently support a link to the Timanides. Group C of Malone et al. [22], sampled from Succession II diamictites, yielded prominent detrital zircon U–Pb age peaks from 990 to 1895 Ma. A subset of much younger ages ranged between 635 and 710 Ma, leading Malone et al. [22] to suggest a distal Timanide source region. Estrada et al. [32] sampled a mica schist from Succession II (sample C11-72) from the eastern margin of Ayles Fiord. This sample yielded a youngest population [$n = 4$] of detrital zircon yielding a concordia age of 572 Ma. In addition, two samples from volcaniclastic sedimentary rocks collected from Succession III yield a weighed mean age [$n = 28$] of c. 573 Ma [32]. Although abundant detrital zircon from Novaya Zemlya and Taimyr ranging from 610–530 Ma [58] provides a sediment pathway to the Timanide orogen, the specific link between Pearya strata and the Timanide Orogen is not well understood.

The Pearya terrane was likely part of a larger continental landmass or amalgamation of crustal fragments that was juxtaposed with the northern Laurentian margin during the Ellesmerian orogeny and served as a sediment source for the southwestward-propagating Devonian Ellesmerian clastic wedge [65]. A distinct population of 500–700 Ma detrital zircon with juvenile Hf isotopic signatures [26, 66, 67] and a shift to more juvenile whole rock Nd isotopic signatures from Devonian siliciclastic units [68] indicate that the northern continental source region had Timanian connections. A number of rock units now distributed across the circum-Arctic and North American Cordillera [53] also yield igneous and detrital zircon ages consistent with a Timanide affinity. Comparisons of these units against the Pearya terrane in general, and Ward Hunt Pluton in particular, provide insight into the possible nature of the Timanian connections prior to the Ellesmerian orogeny.

### Midtkap igneous centers, North Greenland

At its eastern end, the Neoproterozoic–early Devonian passive margin sequence of the Franklinian Basin extends into North Greenland (e.g., [69] and references therein). Most of the Franklinian Basin was deposited above Archean to Paleoproterozoic Laurentian units of the Canadian Shield; however, recent evidence from the Midtkap Igneous Centers in Johannes V. Jensen Land suggests that North Greenland is in part underlain by Timanide crust. The Midtkap Igneous Centers are a group of seven volcanic centers [70,

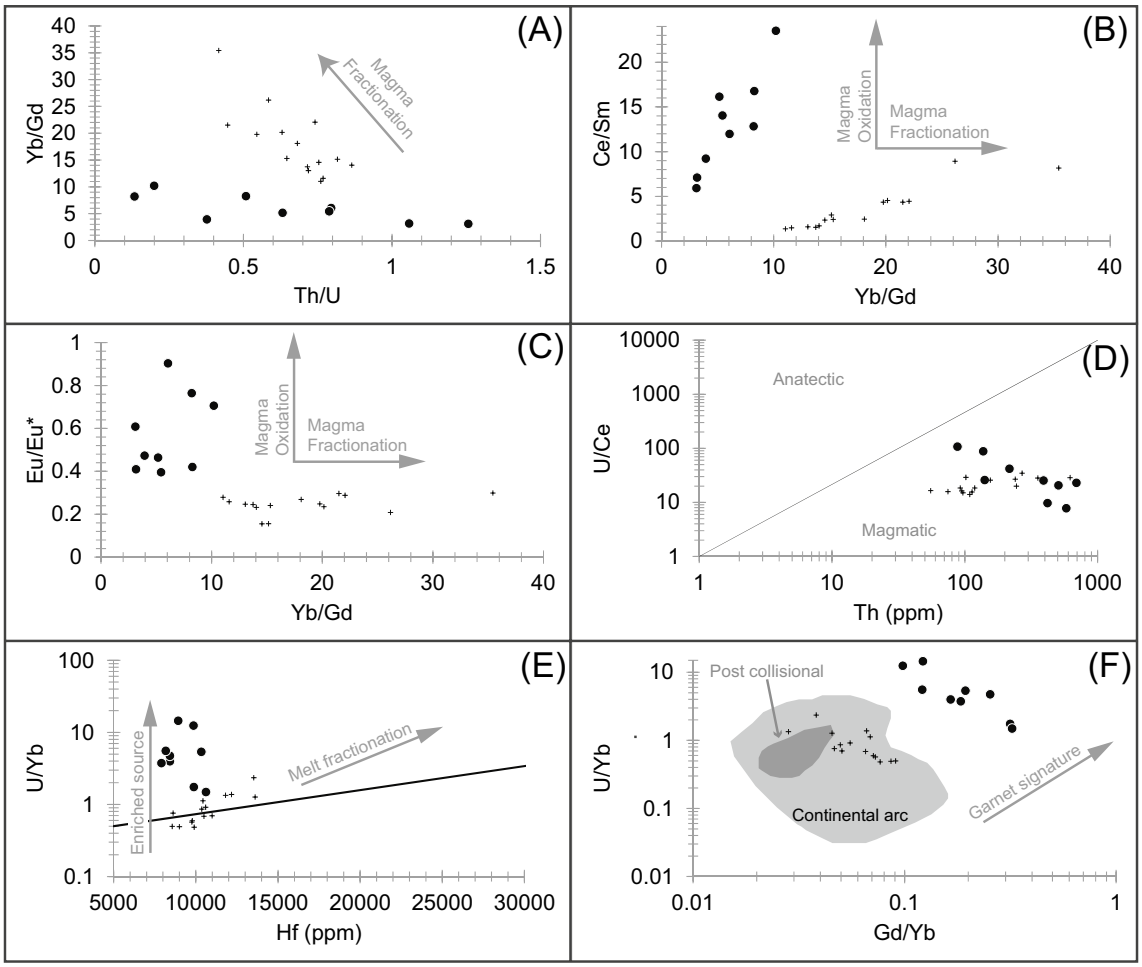


**Fig. 8** Zircon trace-element variation plots including data from the Ward Hunt Pluton (black circles) and zircon standard R33 (black crosses) for comparison. See text for discussion

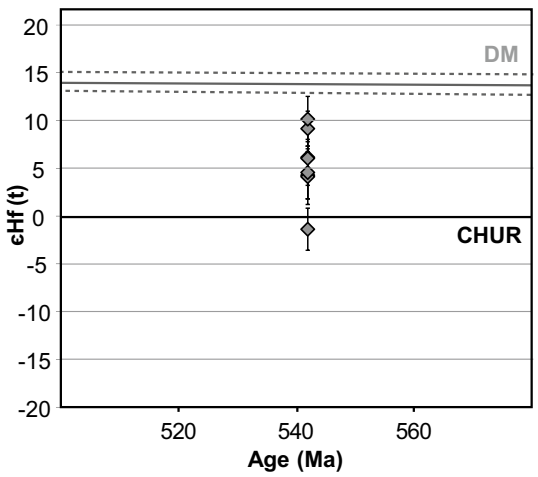


**Fig. 9** Plot of $\varepsilon Hf_{(t)}$ versus the 542 Ma crystallization age for the Ward Hunt Pluton

71] characterized by serpentinized mafic rock emplaced as volcanic breccias into Cambro-Ordovician turbidites [72]. The age of these units is uncertain due to the pervasive serpentinization, although Pedersen and Holm [73] indicated that a K–Ar age of c. 380 Ma reflected a minimum age for the units. The volcanic centers contain xenoliths of unaltered igneous rock which represent the presumed basement to the area [74]. Many xenoliths range in composition from monzonite to granite and bear geochemical indicators of forming in an igneous arc setting [74, 75]. Zircon U–Pb ages from the xenoliths range from c 650 Ma to c. 570 Ma [74, 75]. $^{40}Ar$–$^{39}Ar$ dating of biotite separated from a granite xenolith yielded an age of c. 535 Ma, interpreted by Estrada et al. [75] as documenting island-arc magmatism into the Cambrian. The overlap in these ages suggest that the Ward Hunt Pluton may represent part of the waning stages of arc magmatism in this area, as well, intruded into units that were later emplaced onto the Laurentian margin. Indeed, both Rosa et al. [74] and Estrada et al. [75] suggest that

the Midtkap Igneous Centers basement and the Ward Hunt Pluton are part of the same arc system.

### Arctic Alaska–Chukotka

The Seward Peninsula, centrally located in the Arctic Alaska–Chukotka terrane, provides a rich source of data linking this terrane back to the Timanides. Amato et al. [14, 15] dated abundant late Neoproterozoic orthogneiss units in the Seward Peninsula (Arctic Alaska–Chukotka) as well as a gabbro in the York Mountains. Orthogneiss units collected from the high-grade metamorphic complex exposed in the Kigluaik Mountains ranged in age from c. 700 to c. 562 Ma [14, 15]; in addition, orthogneiss units from the Koolen gneiss dome area of Chukotka yielded ages from c. 581 to c. 562 Ma [15]. These U–Pb ages are consistent with prior work by Patrick and McClelland [13], which yielded an age of c. 680 Ma for Cape Nome and Dorothy Creek orthogneiss units, and the c. 678 Ma Salmon Lake orthogneiss [76]. The York Mountains gabbro yielded a younger U–Pb age of c. 539 Ma [14]. Detrital zircon ages collected from metamorphosed Paleozoic sedimentary rocks show abundant detrital zircon age populations in the 700–540 Ma range [14, 77].

The Doonerak fenster, located in the central Brooks Range of Alaska, offers another Alaskan tie to the Pearya and Alexander terranes and the Timanides. Arc magmatic activity, dated at c. 462 Ma [56], provides a Paleozoic link between Ordovician arc magmatism documented in the Pearya terrane [28, 31, 32] and the Alexander terrane [78]. Detrital zircon from Ordovician sedimentary units of the Apoon Formation in the Doonerak arc include prominent Ordovician peaks, but also include c. 540–520 Ma ages [56]. The authors suggest that these are sourced from outside the assemblage, based on their associations with Proterozoic zircon that yield $\varepsilon Hf_{[t]}$ values consistent with reworked crust. Interestingly, the patterns in age spectra and $\varepsilon Hf_{[t]}$ values permit correlations with data from the Pearya terrane [22, 24]; (this study).

The submerged Chukchi Borderland preserves a record of late Neoproterozoic through Ordovician tectonothermal activity. Rock recovered from dredge samples yielded a suite of quartzofeldspathic gneiss metamorphosed up to granulite facies [79]. Detailed examination of zircon separated from these gneisses revealed complicated metamorphic and resorption textures [80]. U–Pb analyses conducted by O'Brien et al. [80] revealed prolonged zircon growth from c. 550 to c. 470 Ma. Three main age relationships are resolved, with older (c. 550–535 Ma) age domains occurring as chaotically zoned inherited cores, main, sector zoned domains yielding ages between c. 530 and 485 Ma, and younger overgrowth domains and small, euhedral, oscillatory zoned zircon yielding ages of c. 485–420 Ma [80].

### The Alexander terrane

The Alexander terrane has long been recognized as having ties to Baltica and the Timanide and Caledonide orogens, dating back to the late Neoproterozoic to the early Paleozoic (e.g., [16, 17, 54, 56, 81–84]). The basement of the southern Alexander terrane, referred to as the Craig subterrane and exposed on Prince of Wales Island, is composed of metamorphosed arc rocks, including a felsic metavolcanic unit near the base dated by Gehrels et al. [16] at c. 595 Ma and by Oliver et al. [85] at c. 565 Ma. The metavolcanic rocks of the Wales Group are in turn intruded by a c. 554 Ma orthogneiss [86]. The Chilkat Range and Admiralty Island, at the southern margin of the Saint Elias Mountains, has c. 455 Ma felsic plutons with documented c. 547–544 Ma xenocrystic zircon interpreted as being derived from the terrane basement in this region [87]. The new age from the Ward Hunt Pluton overlaps with magmatic activity recorded in the oldest Alexander terrane rocks, providing a further data point supporting ties between the Alexander terrane and the Caledonides through the Pearya terrane. Malone et al. [24] argue for this connection as well, through detrital zircon data collected from early Paleozoic sedimentary rocks compared to Paleozoic rock from across the Alexander terrane [16, 17, 84, 85, 88].

## Conclusions

The Ward Hunt Pluton, intruding metasedimentary rocks of the Pearya terrane, records a previously undocumented late Neoproterozoic–early Cambrian magmatic event in the terrane. Zircon separated from a syenite phase of the pluton yielded a crystallization age of $542 \pm 2$ Ma. Trace-element data from c. 542 Ma zircon record limited magmatic differentiation or crustal input. Hf isotope data reveals a juvenile signature, supporting a paucity of crustal input into the host magma. When taken together, these data suggest that the Ward Hunt Pluton formed in a volcanic arc setting in the Cambrian, allowing for comparisons between it and other Neoproterozoic–Cambrian arc systems. This magmatic event provides further evidence for links between the Pearya terrane and Timanide Orogen, as well as with terranes dispersed around the Circum-Arctic with a record of Timanian magmatism.

**Acknowledgements** Financial support for this study was provided by National Science Foundation Grants EAR-0948359 and EAR-1049368 to McClelland, and EAR 1032156 to the University of Arizona Laserchron Center, Grants from ExxonMobil, and the University of Iowa Department of Earth and Environmental Science to Malone, and funds from Shell Inc. to McClelland. Fieldwork was supported by the Bundesanstalt für Geowissenschaften und Rohstoffe (BGR- German Federal

Institute for Geosciences and Natural Resources). Helpful review by O. Anfinson and J. Majka improved the manuscript.

## References


1. Gee DG, Pease V (2004) The Neoproterozoic Timanide Orogen of eastern Baltica. Geol Soc Lond Mem 30:1–3
2. Pease V, Dovzhikova E, Beliakova L, Gee DG (2004) Late Neoproterozoic granitoid magmatism in the basement to the Pechora Basin, NW Russia: geochemical constrains indicate westward subduction beneath NE Baltica. In: Gee DG, Pease V (eds) The Neoproterozoic Timanide Orogen of Eastern Baltica, vol 30. Geological Society of London Memoir, London, pp 75–85
3. Zonenshain LP, Kuzmin MI, Savostin LA (1990) Geology of the USSR: a plate tectonic synthesis. American Geophysical Union Geodynamics Series, Washington, DC
4. Kuznetsov NB, Soboleva AA, Udoratina OV, Hertseva MV, Andreichev VL (2007) Pre-Ordovician tectonic evolution and volcano-plutonic associations of the Timanides and northern Pre-Uralides, northeast part of the East European Craton. Gondwana Res 12:305–323
5. Kuznetsov NB, Natapov LM, Belousova EA, O'Reilly SY, Griffin WL (2010) Geochronological, geochemical and isotopic study of detrital zircon suites from late Neoproterozoic clastic strata along the NE margin of the East European Craton: Implications for plate tectonic models. Gondwana Res 17:583–601
6. Larinov A, Andraeichev V, Gee D (2004) The Vendian alkaline igneous suite of northern Timan: ion microprobe U/Pb zircon ages of gabbros and syenite. In: Gee DG, Pease V (eds) The Neoproterozoic Timanide Orogen of Eastern Baltica, vol 30. Geological Society of London Memoir, London, pp 69–74
7. Roberts D, Olovyanishnikov V (2004) Structural and tectonic development of the Timanide Orogen. In: Gee DG, Pease V (eds) The Neoproterozoic Timanide Orogen of Eastern Baltica, vol 30. Geological Society of London Memoir, London, pp 47–58
8. Majka J, Mazur S, Manecki M, Czerny J, Holm D (2008) Late Neoproterozoic amphibolite-facies metamorphism of a pre-Caledonian basement block in Wedel Jarsberg Land, Spitsbergen: new evidence from U–Th–Pb dating of monazite. Geol Mag 145:822–830
9. Majka J, Larionov AN, Gee DG, Czerny J, Pršek J (2012) Neoproterozoic pegmatite from Skoddefjellet, Wedel Jarlsberg Land, Spitsbergen: additional evidence for c. 640 Ma tectonothermal event in the Caledonides of Svalbard. Pol Polar Res 33:1–17
10. Majka J, Be'eri-Shlevin Y, Gee DG, Czerny J, Frei D, Ladenberger A (2014) Torellian (c. 640 Ma) metamorphic overprint of Tonian (c. 950 Ma) basement in the Caledonides of southwestern Svalbard. Geol Mag 151:732–748
11. Manecki M, Holm DK, Czerny J, Lux D (1998) Thermochronological evidence for late Proterozoic (Vendian) cooling in southwest Wedel Jarlsberg Land, Spitsbergen. Geol Mag 135:63–69
12. Mazur S, Czerny J, Majka J, Manecki M, Holm D, Smyrak A, Wypych A (2009) A strike-slip terrane boundary in Wedel Jarlsberg Land, Svalbard, and its bearing on correlations of SE Spitzbergen with the Pearya terrane and Timanide belt. J Geol Soc 166:529–544
13. Patrick BE, McClelland WC (1995) Late Proterozoic granitic magmatism on Seward Peninsula and a Barentian origin for Arctic Alaska–Chukotka. Geology 23:81–84
14. Amato JM, Toro J, Miller EL, Gehrels GE, Farmer GL, Gottlieb ES, Till AB (2009) Late Proterozoic–Paleozoic evolution of the Arctic Alaska–Chukotka terrane based on U–Pb igneous and detrital zircon ages: Implications for Neoproterozoic paleogeographic reconstructions. Geol Soc Am Bull 121:1219–1235
15. Amato JM, Aleinikoff JN, Akinin VV, McClelland WC, Toro J (2014) Age, chemistry, and correlations of Neoproterozoic-Devonian igneous rocks of the Arctic Alaska-Chukotka terrane: An overview with new U-Pb ages. In: Dumoulin JA, Till AB (eds) Reconstruction of a Late Proterozoic to Devonian continental margin sequence, Northern Alaska, its paleogeographic significance, and contained base-metal sulfide deposits, vol 506. Geological Society of America Special Paper, Washington, DC, pp 111–131
16. Gehrels GE, Butler RF, Bazard DR (1996) Detrital zircon geochronology of the Alexander terrane, southeastern Alaska. Geol Soc Am Bull 108:722–734
17. White C, Gehrels GE, Pecha M, Giesler D, Yokelson I, McClelland WC (2016) U-Pb and Hf isotope analysis of detrital zircons from Paleozoic strata of the southern Alexander terrane (southeast Alaska). Lithosphere 8:83–96
18. Churkin M Jr, Trexler JH Jr (1980) Continental plates and accreted oceanic terranes. In: Nairn AEM, Churkin M Jr, Stehli FG (eds) The ocean basins and margins: the Arctic Ocean. Plenum Press, New York
19. Trettin HP (1987) Pearya: A composite terrane with Caledonide affinities in northern Ellesmere Island. Can J Earth Sci 24:224–245
20. Trettin HP (1991) Tectonic framework. In: Trettin HP (ed) Geology of the innuitian orogen and arctic platform of Canada and Greenland, vol 3. Geological Survey of Canada, Geology of Canada, Ottawa, pp 59–66
21. Trettin HP (1998) Chapter 4: geology of Pearya. In: Trettin HP (ed) Pre-Carboniferous geology of the northern part of the Arctic Islands, vol 425. Geological Survey of Canada Paper, Ottawa, pp 108–192
22. Malone SJ, McClelland WC, von Gosen W, Piepjohn K (2014) Proterozoic evolution of the North Atlantic–Arctic Caledonides: insights from detrital zircon analysis of metasedimentary rocks from the Pearya Terrane, Canadian High Arctic. J Geol 122:623–648
23. Malone SJ, McClelland WC, von Gosen W, Piepjohn K (2017) The earliest Neoproterozoic magmatic record of the Pearya terrane, Canadian high Arctic: implications for Caledonian terrane reconstructions. Precambr Res 292:323–349
24. Malone SJ, McClelland WC, von Gosen W, Piepjohn K (2019) Detrital zircon U–Pb and Lu–Hf analysis of Paleozoic sedimentary rocks from the Pearya terrane and Ellesmerian Fold Belt (northern Ellesmere Island): a comparison with Circum-Arctic datasets and their implications on terrane tectonics. In: Piepjohn K, Strauss JV, Reinhardt L, McClelland WC (eds) Circum-Arctic structural events: tectonic evolution of the arctic margin and trans-Arctic links with adjacent orogens, vol 541. Geological Society of America Special Paper, Washington, DC, pp 231–254
25. Trettin HP (1991) Silurian-early Carboniferous deformational phases and associated metamorphism and plutonism, Arctic Islands. In: Trettin HP (ed) Geology of the Innuitian Orogen and Arctic Platform of Canada and Greenland, vol 3. Geological Survey of Canada, Geology of Canada, Ottawa, pp 295–341
26. Anfinson OA, Leier AL, Gaschnig R, Embry AF, Dewing K (2012) U-Pb and Hf isotopic data from Franklinian Basin strata: insights into the nature of Crockerland and the timing of accretion, Canadian Arctic Islands. Can J Earth Sci 49:1316–1328
27. Ward WP, McClelland WC, Coble MA, Malone SJ (2015) Timing of deformation and metamorphism in the Pearya terrane from SIMS analysis of monazite and titanite. Geol Soc Am Abstr Progr 47:26–44
28. Trettin HP, Parrish R, Loveridge WD (1987) U-Pb age determinations of Proterozoic to Devonian rocks from northern Ellesmere Island, Arctic Canada. Can J Earth Sci 24:246–256
29. Trettin HP (1991) The Proterozoic to late Silurian Record of Pearya. In: Trettin HP (ed) Geology of the innuitian orogen and

Arctic platform of Canada and Greenland, vol 3. Geological Survey of Canada, Geology of Canada, Ottawa, pp 241–259
30. von Gosen W, Piepjohn K, McClelland WC, Läufer A (2012) The Pearya Shear Zone in the Canadian High Arctic: kinematics and significance. Zeitschrift der Deutschen Gesellschaft für Geowissenschaften (Ger J Geosci) 163:233–249
31. Trettin HP, Parrish RR, Roddick JC (1992) New U-Pb and $^{40}$Ar-$^{39}$Ar age determinations from northern Ellesmere and Axel Heiberg islands, Northwest Territories and their tectonic significance. Geol Surv Can Pap 92–2:3–30
32. Estrada S, Mende K, Gerdes A, Gärtner A, Hofmann M, Spiegel D, Damaske D, Koglina N (2018) Proterozoic to Cretaceous evolution of the western and central Pearya Terrane (Canadian High Arctic). J Geodyn 120:45–76
33. Trettin HP, Loveridge WD, Sullivan RW (1982) U–Pb ages on zircons from the M'Clintock West massif and the Markham Fiord pluton, northernmost Ellesmere Island. Geol Surv Can Pap 82-1C:161–166
34. Okulitch AV (1991) Chapter 12. Silurian–Early Carboniferous deformational phases and associated metamorphism and plutonism, Arctic Islands. F. Late Devonian–Early Carboniferous deformation of the Central Ellesmere and Jones Sound fold belts. In: Trettin HP (ed) Geology of the Innuitian Orogen and Arctic Platform of Canada and Greenland, vol 3. Geological Survey of Canada, Geology of Canada, Ottawa, pp 318–320
35. Soper NJ, Higgins AK (1991) Deformation (Devonian– Early Carboniferous deformation and metamorphism, North Greenland). In: Trettin HP (ed) Geology of the Innuitian Orogen and Arctic Platform of Canada and Greenland, vol 3. Geological Survey of Canada, Geology of Canada, Ottawa, pp 283–288
36. Mayr U, de Freitas T, Beauchamp B, Eisbacher G (1998) The Geology of Devon Island north of 76°, Canadian Arctic Archipelago. Geol Surv Can Bull 526:1–500
37. Piepjohn K, von Gosen W, Läufer A, McClelland WC, Estrada S (2013) Ellesmerian and Eurekan fault tectonics at the northern margin of Ellesmere Island (Canadian High Arctic). Zeitschrift der Deutschen Gesellschaft für Geowissenschaften (Ger J Geosci) 164:81–105
38. Piepjohn K, von Gosen W, Tessensohn F, Reinhardt L, McClelland WC, Dallmann W, Gaedicke C, Harrison JC (2015) Tectonic map of the Ellesmerian and Eurekan deformation belts on Svalbard, North Greenland, and the Queen Elizabeth Islands (Canadian Arctic). Arktos 1:1–12
39. Frisch T (1974) Metamorphic and plutonic rocks of northernmost Ellesmere Island, Canadian Arctic Archipelago. Geol Surv Can Bull 229:1–87
40. Barth AP, Wooden JL (2010) Coupled elemental and isotopic analyses of polygenetic zircons from granitic rocks by ion microprobe, with implications for melt evolution and the sources of granitic magmas. Chem Geol 227:149–159
41. Black LP, Kamo SL, Allen CM, Davis DW, Aleinikoff JN, Valley JW, Mundil R, Campbell IH, Korsch RJ, Williams IS, Foudoulis C (2004) Improved 206Pb/238U microprobe geochronology by the monitoring of a trace-element-related matrix effect; SHRIMP, ID–TIMS, ELA–ICP–MS and oxygen isotope documentation for a series of zircon standards. Chem Geol 205:115–140
42. Mattinson JM (2010) Analysis of the relative decay constants of $^{235}$U and $^{238}$U by multi-step CA-TIMS measurements of closed-system natural zircon sample. Chem Geol 275:186–198
43. Coble MA, Vasquez JA, Barth AP, Wooden J, Burns D, Kylander-Clark A, Jackson S, Vennari CE (2018) Trace element characterisation of MAD-559 zircon reference material for ion microprobe analysis. Geostand Geoanal Res. https://doi.org/10.1111/ggr.12238
44. Ludwig KR (2005) Squid version 1.13b: a user's manual. Berkley Geochronol Cent Spec Publ 2:1–22
45. Ludwig KR (2003) User's manual for Isoplot 3.00: a geochronological toolkit for Microsoft Excel. Berkley Geochronol Cent Spec Publ 4:1–70
46. Gehrels GE, Valencia V, Pullen A (2006) Detrital zircon geochronology by laser-ablation multicollector ICPMS at the Arizona Laserchron Center. Paleontol Soc Pap 12:67–76
47. Gehrels GE, Valencia VA, Ruiz J (2008) Enhanced precision, accuracy, efficiency and spatial resolution of U–Pb ages by laser ablation-multicollecter-inductively coupled plasma-mass spectrometry. Geochem Geophys Geosyst 9:1–13
48. Cecil MR, Gehrels G, Ducea MN, Patchett PJ (2011) U–Pb–Hf characterization of the central Coast Mountains batholith: implications for petrogenesis and crustal architecture. Lithosphere 3:247–260
49. Hoskin PWO, Schaltegger U (2003) The composition of zircon and igneous and metamorphic petrogenesis. In Hanchar JM, Hoskin PW (eds) Zircon. Reviews in minerology and geochemistry 53:27–62
50. Griffin WL, WangX JSE, Pearson NJ, O'Reilly SY, Xu X, Zhou X (2002) Zircon chemistry and magma mixing, SE China: in-situ analysis of Hf isotopes, Tonglu and Pingtan igneous complexes. Lithos 61:237–269
51. Breiter K, Lamarao CN, Borges RMK, Dall'Agnol R (2014) Chemical characteristics of zircon from A-type granites and comparison to zircon of S-type granites. Lithos 192–195:208–225
52. Grimes CB, Cheadle MJ, Wooden JL, John BE (2015) "Fingerprinting" tectono-magmatic provenance using trace elements in igneous zircon. Contrib Min Pet 170:46
53. Colpron M, Nelson J (2009) A Paleozoic Northwest Passage: incursion of Caledonian, Baltican and Siberian terranes into eastern Panthalassa, and the early evolution of the North American Cordillera. In: Cawood PA, Kroner A (eds) Earth accretionary systems in space and time, vol 318. Geological Society of London Special Publications, London, pp 273–307
54. Beranek LP, van Staal CR, Gordee SM, McClelland WC, Israel S, Mihalynuk M (2012) Tectonic significance of upper Cambrian–middle Ordovician mafic volcanic rocks on the Alexander terrane, Saint Elias Mountains, northwestern Canada. J Geol 120:293–314
55. Miller EL, Kuznetsov N, Soboleva A, Udoratina O, Grove MJ, Gehrels G (2011) Baltica in the Cordillera? Geology 39:791–794
56. Strauss JV, Hoiland CW, Ward WP, Johnson BG, Nelson LL, McClelland WC (2017) Orogen transplant: Taconic–Caledonian arc magmatism in the central Brooks Range of Alaska. Geol Soc Am Bull 129:649–676
57. Lorenz H, Gee DG, Simonetti A (2008) Detrital zircon ages and provenance of the Late Neoproterozoic and Palaeozoic successions on Severnaya Zemlya, Kara Shelf: a tie to Baltica. Nor J Geol 88:235–258
58. Pease V, Scott RA (2009) Crustal affinities in the Arctic Uralides, northern Russia: significance of detrital zircon ages from Neoproterozoic and Palaeozoic sediments in Novaya Zemlya and Taimyr. J Geol Soc 166:517–527
59. Lorenz H, Gee DG, Korago E, Kovaleva G, McClelland WC, Gilotti JA, Frei D (2013) Detrital zircon geochronology of Palaeozoic Novaya Zemlya—a key to understanding the basement of the Barents Shelf. Terra Nova 25:496–503
60. Ershova VB, Lorenz H, Prokopiev AV, Sobolev NN, Khudoley AK, Petrov EO, Estrada S, Sergeev S, Larionov A, Thomsen TB (2016) The De Long Islands: a missing link in unraveling the Paleozoic paleogeography of the Arctic. Gondwana Res 35:305–322
61. Ershova VB, Prokopiev AV, Khudoley AK, Petrov EO, Andersen T, Kullerud K, Kolchanov DA (2020) U-Pb Age and Hf Isotope Geochemistry of Detrital Zircons from Cambrian Sandstones of the Severnaya Zemlya Archipelago and Northern Taimyr (Russian High Arctic). Minerals 10:36

62. McClelland WC, Malone SJ, von Gosen W, Piepjohn K, Läufer A (2012) The timing of sinistral displacement of the Pearya Terrane along the Canadian Arctic Margin. Zeitschrift der Deutschen Gesellschaft für Geowissenschaften (Ger J Geosci) 163:251–259
63. Majka J, Kośmińska K, Mazur S, Czerny J, Piepjohn K, Dwornik M, Manecki M (2015) Two garnet growth events in polymetamorphic rocks in southwest Spitsbergen, Norway: insight in the history of Neoproterozoic and early Paleozoic metamorphism in the High Arctic. Can J Earth Sci 52:1045–1061
64. Ohta Y (1994) Caledonian and Precambrian history in Svalbard: a review and implication of escape tectonics. Tectonophysics 231:183–194
65. Embry AF (1988) Middle–Upper Devonian sedimentation in the Canadian Arctic Islands and the Ellesmerian orogeny. In: MacMillan NJ, Embry AF, Glass DJ (eds) Devonian of the World, vol 14. Canadian Society of Petroleum Geologists Memoir, Ottawa, pp 15–28
66. Anfinson OA, Leier AL, Embry AF, Dewing K (2012) Detrital zircon geochronology and provenance of the Neoproterozoic to Late Devonian Franklinian Basin, Canadian Arctic Islands. Geol Soc Am Bull 124:415–430
67. Anfinson OA, Leier AL, Dewing K, Guest B, Stockli DF, Embry AF (2013) Insights into the Phanerozoic tectonic evolution of the northern Laurentian margin: detrital apatite and zircon (U–Th)/He ages from Devonian strata of the Franklinian Basin, Canadian Arctic Islands. Can J Earth Sci 50:761–768
68. Patchett PJ, Roth MA, Canale BS, de Freitas TA, Harrison JC, Embry AF, Ross GM (1999) Nd isotopes, geochemistry, and constraints on sources of sediments in the Franklinian mobile belt, Arctic Canada. Geol Soc Am Bull 111:578–589
69. Henriksen N, Higgins AK, Karlsbeek F, Pulvertaft TCR (2009) Greenland from Archean to Quaternary. Descriptive text to the 1995 Geological map of Greenland, 1:2,500,000. Geol Surv Den Greenland Bull 18:126
70. Pedersen SAS (1980) Regional geology and thrust fault tectonics in the southern part of the North Greenland fold belt, North Peary Land. Rapport Grønlands Geologiske Undersøgelse 99:79–87
71. Soper NJ, Higgins AK, Friderichsen JD (1980) The North Greenland fold belt in eastern Johannes V. Jensen Land. Rapport Grønlands Geologiske Undersøgelse 99:89–98
72. Parsons I (1981) Volcanic centres between Frigg Fjord and Midtkap, eastern North Greenland. Rapport Grønlands Geologiske Undersøgelse 106:69–75
73. Pedersen SAS, Holm M (1983) The significance of a Middle Devonian K/Ar age of an intrusive rock in the southern part of the North Greenland Fold Belt. Bull Geol Soc Den 31:121–127
74. Rosa D, Majka J, Thrane K, Guarnieri P (2016) Evicence for Timianian-age basement rocks in North Greenland as documented through U–Pb zircon dating of igneous xenoliths from the Midtkap volcanic centers. Precambr Res 275:394–405
75. Estrada S, Tessensohn F, Benita-Lissete S (2018) A Timanian island-arc fragment in North Greenland: the Midtkap igneous suite. J Geodyn 118:140–153
76. Amato JM, Wright JE (1998) Geochronologic investigations of magmatism and metamorphism within the Kigluaik Mountains gneiss dome, Seward Peninsula, Alaska. In: Clough JG, Larson F (eds) Short Notes on Alaska Geology 1997, vol 118. Alaska Division of Geological and Geophysical Surveys Prof Rep, Fairbanks, pp 1–22
77. Till AB, Amato JM, Aleinikoff JN, Bleick HA (2014) U-Pb detrital zircon geochronology as evidence for the origin of the Nome Complex, northern Alaska, and implications for regional and trans-Arctic correlations. In: Dumoulin JA, Till AB (eds) Reconstruction of a Late Proterozoic to Devonian continental margin sequence, Northern Alaska, its paleogeographic significance, and contained base-metal sulfide deposits, vol 506. Geological Society of America Special Paper, Washington, DC, pp 111–131
78. Gehrels GE, Saleeby JB (1987) Geologic framework, tectonic evolution, and displacement history of the Alexander terrane. Tectonics 6:151–173
79. Brumley K, Miller EL, Konstantinou A, Grove M, Meisling KE, Mayer LA (2015) First bedrock samples dredged from submarine outcrops in the Chukchi Borderland, Arctic Ocean. Geosphere 11:76–92
80. O'Brien T, Miller EL (2014) Continuous zircon growth during long-lived granulite facies metamorphism: a microtextural, U–Pb, Lu–Hf, and trace element study of Caledonian rocks from the Chukchi Borderland, Arctic Ocean. Contr Min Pet 168:1–19
81. Soja CM (1994) Significance of Silurian stromatolite–sphinctozoan reefs. Geology 22:355–358
82. Bazard DR, Butler RF, Gehrels GE, Soja CM (1995) Paleomagnetism of the Early Devonian Karheen Formation, southeast Alaska: implication for the Alexander terrane paleogeography. Geology 23:707–710
83. Beranek LP, van Staal CR, McClelland WC, Israel S, Mihalynuk MG (2013) Baltican crustal provenance for Cambrian–Ordovician sandstones of the Alexander terrane, North American Cordillera: evidence from detrital zircon U–Pb geochronology and Hf isotope geochemistry. J Geol Soc 170:7–18
84. Beranek LP, van Staal CR, McClelland WC, Israel S, Mihalynuk MG (2013) Detrital zircon Hf isotopic compositions indicate a northern Caledonian connection for the Alexander terrane. Lithosphere 5:163–168
85. Oliver J, Roberts K, Friedman R (2011) The Niblack mine: a Neoproterozoic precious metals enhanced, volcanic hosted massive sulfide, Prince of Wales Island Alaska. Mineralized zones and mineral resources, structural style, stratigraphic and U–Pb geochronological relationships. Alaska Miners Association of Annual Convention of Abstracts, pp 60–62
86. Gehrels GE (1990) Late Proterozoic–Cambrian metamorphic basement of the Alexander Terrane on Long and Dall Islands, southeast Alaska. Soc Am Bull 102:760–767
87. Karl SM, Haeussler PJ, Friedman RM, Mortensen JK, Himmelberg GR, Zumsteg CL (2006) Late Proterozoic ages for rocks on Mount Cheetdeekahyu and Admiralty Island, Alexander terrane, southeast Alaska. Geol Soc Am Abstr Progr 38:20
88. Tochilin C, Gehrels GE, Nelson J, Mahoney B (2014) U-Pb and Hf isotope analysis of detrital zircons from the Banks Island assemblage (coastal British Columbia) and southern Alexander terrane (southeast Alaska). Lithosphere 6:200–215
89. Mayr U (1992) Reconnaissance and preliminary interpretation of Upper Devonian to Permian stratigraphy of northeastern Ellesmere Island, Canadian Arctic Archipelago. Geol Surv Can Pap 91–08:122